

Red/NIR-Emissive Benzo[d]imidazole-Cored AIEgens: Facile Molecular Design for Wavelength Extending and In Vivo Tumor Metabolic Imaging

Jen-Shyang Ni, Pengfei Zhang, Tao Jiang, Yuncong Chen, Huifang Su, Dong Wang, Zhen-Qiang Yu, Ryan T. K. Kwok, Zujin Zhao, Jacky W. Y. Lam, and Ben Zhong Tang*

Aggregation-induced emission (AIE) luminogens (AIEgens) with red/near-infrared (NIR) emissions are appealing for applications in optoelectronics and biomedical engineering owing to their intrinsic advantages of efficient solid-state emission, low background, and deep tissue penetration. In this context, an AIEgen with long-wavelength emission is synthesized by introducing tetraphenylethene (TPE) to the periphery of electron-deficient *spiro*-benzo[d]imidazole-2,1'-cyclohexane (BI). The resulting AIEgen, abbreviated as 2TPE-BI, adopts a donor–acceptor structure and shows bathochromic absorption and emission with a larger Stokes shift of 157 nm in acetonitrile than that based on benzo[c][1,2,5]thiadiazole. It also exhibits a high solid-state fluorescence quantum yield of 56.6%. By further insertion of thiophene to its molecular structure generates 2TPE-2T-BI with higher conjugation and NIR emission. 2TPE-2T-BI can be fabricated into AIE dots for in vivo metabolic labeling through bio-orthogonal click chemistry. These results open a new approach for facile construction of long-wavelength emissive AIEgens based on the BI core.

biological imaging,^[3] owing to their deep tissue penetration, less biological photo-damage, and minimum interference from background autofluorescence of biomolecules in living systems.^[4] To date, this is still of great demand to develop new long-wavelength emissive fluorophores. Lengthening the π -electron system has been recognized as one of the general design strategy to develop fluorescent materials with long wavelength absorbing or emitting, for example, oligo-olefins and polymethine dyes.^[4a,5] However, these conventional fluorophores possess thermal and photochemical instability, small Stokes shift, high interference from the excitation light and/or self-absorption, and aggregation-caused quenching (ACQ) effect (strong emission in dilute solution but quenching upon the concentration increased due to their strong intermolecular π – π interactions). All these respective

Molecular construction of organic π -conjugated materials owning long-wavelength emissive properties has been of great demand and potential applications in the photoelectronic devices, such as organic light-emitting diodes^[1] and luminescent solar concentrator.^[2] More importantly, long-wavelength emissive fluorescent materials have many prominent merits in

and collective drawbacks limit their biomedical applications.^[6]

The donor–acceptor (D–A) architecture has been a broadly adopted strategy for designing the long-wavelength emissive molecules,^[7] whereby electron-donating and electron-withdrawing segments are incorporated into the molecular backbone.^[8] After the molecular orbitals (MOs) of the conjugated


Dr. J.-S. Ni, Dr. P. Zhang, Dr. Y. Chen, Dr. H. Su, Prof. R. T. K. Kwok, Prof. J. W. Y. Lam, Prof. B. Z. Tang
HKUST-Shenzhen Research Institute
No. 9 Yuexing 1st RD, South Area
Hi-tech Park, Shenzhen 518057, China
E-mail: tangbenz@ust.hk

Dr. P. Zhang, Dr. Y. Chen, Dr. H. Su, Prof. R. T. K. Kwok, Prof. J. W. Y. Lam, Prof. B. Z. Tang
Department of Chemistry
Hong Kong Branch of Chinese National Engineering Research Center for Tissue Restoration and Reconstruction
Institute for Advanced Study and Division of Life Science
Hong Kong University of Science and Technology
Clear Water Bay, Kowloon, Hong Kong

Dr. P. Zhang, T. Jiang
Guangdong Key Laboratory of Nanomedicine
Shenzhen Engineering Laboratory of Nanomedicine and Nanoformulations
CAS Key Laboratory of Health Informatics
Institute of Biomedicine and Biotechnology
Shenzhen Institutes of Advanced Technology
Chinese Academy of Sciences
Shenzhen 518055, China

Prof. D. Wang, Prof. Z.-Q. Yu
Center for AIE Research
College of Materials Science and Engineering
Shenzhen University
Shenzhen 518060, China

Prof. Z. Zhao, Prof. B. Z. Tang
SCUT-HKUST Joint Research Laboratory
State Key Laboratory of Luminescent Materials and Devices
South China University of Technology
Guangzhou 510640, China

 The ORCID identification number(s) for the author(s) of this article can be found under <https://doi.org/10.1002/adma.201805220>.

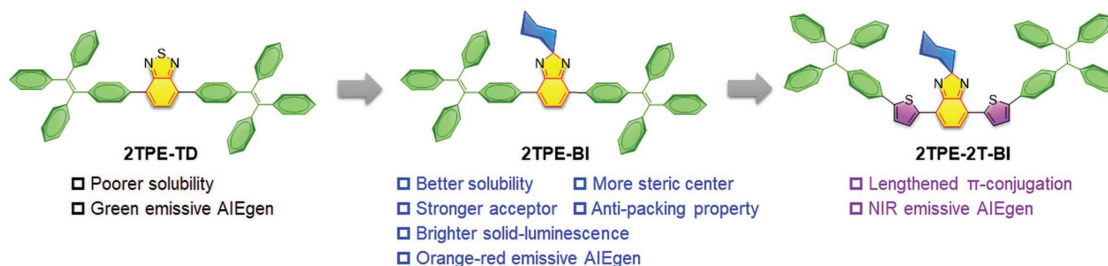
DOI: 10.1002/adma.201805220

donor and acceptor mixed, the new formation of hybridized MOs with an effective and narrowed bandgap (E_g) can be achieved, leading to the redshifting absorption and emission.^[8a] Among them, benzo[c][1,2,5]thiadiazole (TD)^[9] is the one of most typical low-bandgap acceptor, and its excellent photo-/thermostable properties have been applied broadly in the optoelectronics and biological imaging. With great efforts of scientists across several disciplines, a series of special electron-deficient heterocycles based on TD structure have been developed such as benzo[1,2-*c*:4,5-*c'*]bis[1,2,5]thiadiazole,^[4c,10] naphtho[2,3-*c*][1,2,5]thiadiazole,^[11] naphtho[1,2-*c*:5,6-*c'*]bis[1,2,5]thiadiazole,^{[12][1,2,5]}thiadiazolo[3,4-*g*]quinoxaline,^[10a,13] 2,1,3-benzothiadiazole-5,6-dicarboxylicimide,^[14] 7-alkyl-6*H*-pyrrolo[3,4-*b*][1,2,5]thiadiazolo[3,4-*g*]quinoxaline-6,8(7*H*)-dione,^[15] and so forth (Scheme S1, Supporting Information). Though TD-based heterocycles have advantages of strong electron-withdrawing ability and bathochromic absorption and emission spectra, the extremely complex synthetic routes, poor solubility, hard purification and low yield still limited their further molecular modification and development. Thus, we wonder whether the electron-rich sulfur atom of TD acceptor could be replaced with electron-poor atom, such as boron and carbon atoms, to enhance the electron-withdrawing ability and modify with a steric substitution simultaneously. Fortunately, we found that the quinoid form of 2*H*-benzo[d]imidazole showed lower bandgap energy than TD unit according to the calculated results with time-dependent density functional theory (TD-DFT) as the level of B3LYP/6-31G* (Figure S1, Supporting Information). In addition, its second-position carbon atom can be substituted with alkyl-chains, which can directly increase molecular solubility without the influence of conjugation on molecular framework and be helpful for material purification. The 2*H*-benzo[d]imidazole-based conjugated polymers had been applied in organic photovoltaics in terms of the advantages of good carrier and hole mobilities, good solubility and high thermal stability.^[16]

In this investigation, we thus will attempt to incorporate BI moiety into the D–A type aggregation-induced emission (AIE) luminogens (AIEgens), which is dim emissive in the dissolution state but strong in aggregation or solid states,^[17] to achieve long-wavelength emission with high quantum efficiency. As shown in **Scheme 1**, the BI-based AIEgen (2TPE-BI) is composed of i) AIE-active tetraphenylethene (TPE) unit as donor, ii) strong electron-withdrawing BI moiety as core, and iii) steric cyclohexane as bulky substitution against the intermolecular π – π stacking and increasing molecular solubility. Compared to our previous AIEgen based on TD acceptor (2TPE-TD),^[9a] 2TPE-BI luminogen showed redshifting absorption and

emission about 44–53 nm in solution, better AIE performance and brighter orange–red solid-luminescence at 617 nm wavelength with 56.6% of absolute quantum efficiency, which was attributed to the synergistic interaction of electron-deficient quinoidal BI acceptor and intermolecular antistacking *spiro*-cyclohexane substituent. After inserted with thiophene into the skeleton of 2TPE-BI luminogen, the NIR emissive AIEgen (2TPE-2T-BI) was developed. Further fabricating 2TPE-2T-BI into clickable NIR AIEdots,^[18] abbreviated dibenzocyclooctyl (DBCO)-AIEdots, these could bio-orthogonally conjugated with azido groups in biological environment.^[19] As far as clinical science, the implementation of highly sensitive and specific imaging modalities for timely cancer diagnosis and progression monitoring has been of great significance. Traditionally, the endogenous target molecules on live cells can be visualized using different binding molecules labeled with imaging probes such as antibodies, peptides, or aptamers. However, the low amount of target molecules on cell surface limited the efficacy of molecular imaging *in vivo*.^[20] Bio-orthogonal chemistry has shown powerful applications in biological fields in combination with metabolic glycoengineering. Through the intrinsic metabolism of metabolic glycoengineering, unnatural glycans are introduced onto cells by feeding specific precursors, tetraacetylated *N*-azidoacetyl- β -mannosamine (Ac4ManNAz) containing particular azido-groups. Therefore, after DBCO-AIEdots were intravenously injected into tumor-bearing mice, the cancer cell surface labeling with unnatural sialic acids could be specifically targeted by chemically binding of *in vivo* biorthogonal copper-free click chemistry.

First of all, in the material synthesis, the novel AIEgens (2TPE-BI and 2TPE-2T-BI) were synthesized through palladium-catalyzed Stille coupling reaction of 4,7-dibromo-*spiro*[benzo[d]imidazole-2,1'-cyclohexane] (Br-BI-Br)^[21] and stannane derivatives as illustrated in Scheme S2 of the Supporting Information, and further characterized by nuclear magnetic resonance spectroscopy and high-resolution mass spectrometry with satisfactory results. Both thermogravimetric analyses showed good thermal stability over 400 °C (Figure S2, Supporting Information), which is comparable with 2TPE-TD (429 °C).^[9a] With the purpose of relating the photophysical properties between BI and TD-based materials, UV–vis absorption and photoluminescence (PL) spectra of 2TPE-BI and 2TPE-TD in tetrahydrofuran (THF) at a concentration of 10×10^{-6} M were measured as shown in **Figure 1A** and **Figure S3** (Supporting Information), and the corresponding data were listed in **Table 1**. The high-energy absorption peaks below 350 nm arose from π – π^* transitions, and the low-energy peaks at



Scheme 1. Design strategy of quinoidal AIEgens based on benzo[d]imidazole acceptor and antistacking *spiro*-cyclohexane substituent.

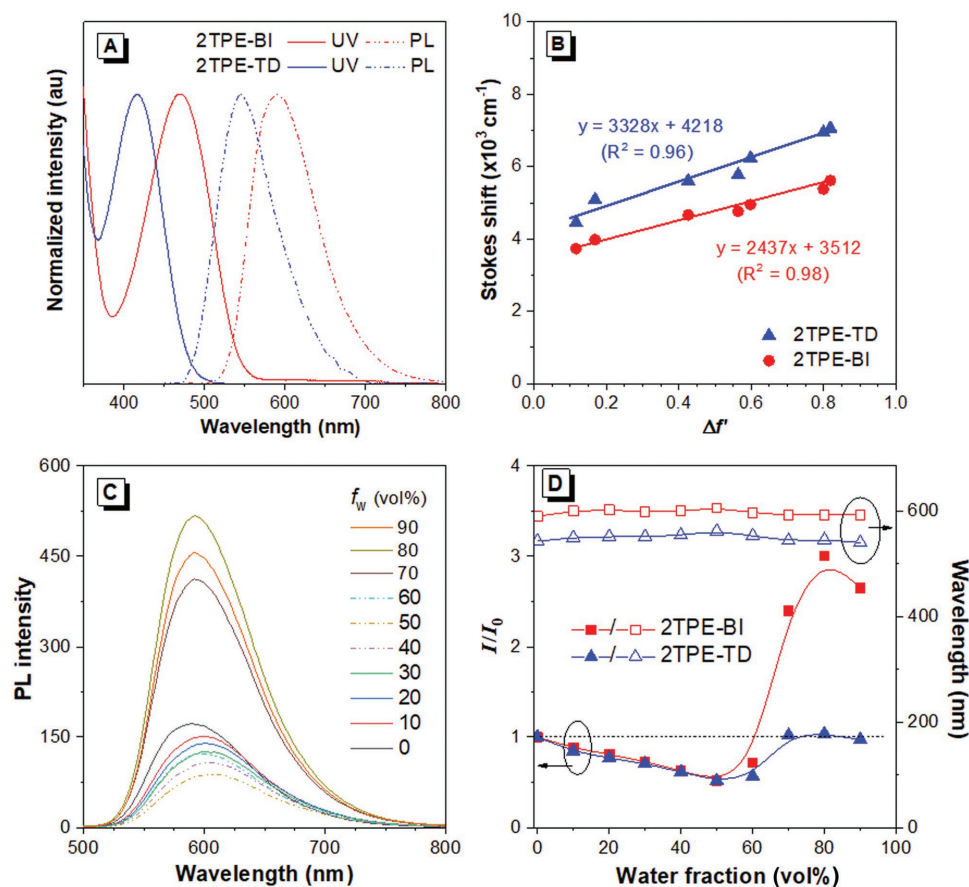


Figure 1. A) Normalized UV-vis absorption and PL spectra in THF ($10 \times 10^{-6} \text{ M}$), B) the revised Lippert–Mataga plots versus orientation polarizability (Δf), C) PL spectra of 2TPE-BI in the different water fractions (f_w vol%), and D) plots of AIE curves and their corresponding maximum emission wavelength in the different water fractions (vol%).

417 and 470 nm were attributed to the intramolecular charge-transfer (ICT) transition from TPE segment to the acceptor mixed with π – π^* character according to the calculated results (Table S1, Supporting Information). Compared with 2TPE-TD, 2TPE-BI had more bathochromic shift in the absorption and emission spectra about 53 and 44 nm (Figure 1A and Table 1, and Tables S1 and S2 in the Supporting Information), respectively, resulting from that the stronger electron-withdrawing capability of BI core diminished the energy gap between the highest occupied molecular orbital (HOMO) and the lowest unoccupied molecular orbital (LUMO) in good agreement

with the calculated results (vide infra). However, both of the revised Lippert–Mataga slopes (Figure 1B), the plot of Stokes shift versus the orientation polarizability (Δf),^[22] were close as a consequence of the similar difference values of dipole moments ($\Delta\mu$) between the ground and excited states (0.30 D for 2TPE-BI and 0.46 D for 2TPE-TD; Figure S4 and Table S3, Supporting Information),^[23] implying that both luminogens have the comparable ICT process and solvatochromism effects (Figure S5 and Table S4, Supporting Information).

To gain the insight into AIE characteristic, the fluorescent properties in a mixture of THF and water were investigated

Table 1. Photophysical properties of 2TPE-TD, 2TPE-BI, 2TPE-2T-TD, and 2TPE-2T-BI.

	THF ^{a)}					Solid powder ^{f)}		$\alpha_{\text{AIE}}^g)$
	λ_{abs} (log ϵ) [nm]	λ_{em} (Φ) [nm, %] ^{b)}	τ (k_r , k_{nr}) [ns, ns ^{−1} , ns ^{−1}] ^{c)}	Δ_{THF} [nm] ^{d)}	E_g [eV] ^{e)}	λ_{em} (Φ) [nm, %]	τ (k_r , k_{nr}) [ns, ns ^{−1} , ns ^{−1}]	
2TPE-TD	417 (4.45)	544 (64.6)	3.77 (0.171, 0.094)	127	2.55	545 (45.8)	2.50 (0.183, 0.217)	0.7
2TPE-BI	470 (4.35)	588 (14.1)	1.80 (0.078, 0.477)	118	2.30	617 (56.6)	6.91 (0.082, 0.063)	4.0
2TPE-2T-TD	510 (4.63)	625 (68.0)	4.98 (0.137, 0.064)	113	2.05	672 (2.3)	0.91 (0.025, 1.069)	0.03
2TPE-2T-BI	562 (4.61)	677 (42.8)	3.92 (0.109, 0.146)	115	1.96	767 (0.5)	0.76 (0.007, 1.309)	0.01

^{a)}Recorded in THF at 298 K ($10 \times 10^{-6} \text{ M}$); ^{b)}Quantum yield (Φ) was measured with absolute method; ^{c)}Rate constants for radiative (k_r) and nonradiative decay (k_{nr}) were calculated from Φ and lifetime (τ) values according to $k_r = \Phi/\tau$ and $k_{nr} = (1 - \Phi)/\tau$; ^{d)}Stokes shift, $\Delta_{\text{THF}} = \lambda_{\text{em}} - \lambda_{\text{abs}}$; ^{e)}Bandgap (E_g) calculated from the intersection of absorption and emission spectra; ^{f)}Measured with powder; ^{g)} $\alpha_{\text{AIE}} = \Phi_{\text{solid}}/\Phi_{\text{THF}}$.

(Figure 1C,D, Figures S6 and S7 in the Supporting Information). 2TPE-BI in pure THF solution emits orange fluorescence (590 nm). Upon the increase of water fraction (f_w) from 0 to 50 vol%, PL intensities were weakened gradually, and their emission peaks were red-shifted to 606 nm along with the increase of solvent polarity, which is the representative twisted intramolecular charge transfer (TICT) effect.^[24] Upon further increase of f_w , the intensities started to rise and their wavelength were blue-shifting to 593 nm, arising from that the aggregation formation causes AIE character. In comparison with 2TPE-TD, 2TPE-BI behaved the similar TICT feature due to the alike solvatochromism effect (vide supra) but better AIE performance in high f_w environment. The ratios between the intensities of 80 and 50 vol% f_w were 5.84 and 2.01 for 2TPE-BI and 2TPE-TD, respectively. The better AIE performance of 2TPE-BI can be attributed to the stronger inhibition of the intermolecular π - π stacking by cyclohexyl-chain substitution.

According to the time-resolved fluorescence spectra (Figure S8, Supporting Information), the fluorescence lifetime of 2TPE-BI in THF was 1.80 ns and shorter than that of 2TPE-TD (3.77 ns), whereas the former was larger than the latter (6.91 vs 2.51 ns) in the solid state. Their radiative and nonradiative decay rates (k_r and k_{nr}) were further expressed and listed in Table 1. In THF, the nonradiative decay rate (477 ps^{-1}) of 2TPE-BI was larger than the radiative decay rate (78 ps^{-1}) by six times, whereas these values of 2TPE-TD were the same

order of magnitude ($171 \text{ vs } 94 \text{ ps}^{-1}$ for k_r vs k_{nr}). The main reason why 2TPE-BI had more nonradiative decay channel in THF was the more intramolecular motions and its lower adiabatic excitation energy (E_{ad} ; vide infra of theoretical calculation).^[25] However, in solid, the k_{nr} value of 2TPE-BI decreased drastically to 63 ps^{-1} and was slightly lower than the k_r value (82 ps^{-1}). The results suggested that nonradiative decay was dominant for 2TPE-BI in solution but weakened to the same level as radiative decay in solid, i.e., the ratio of nonradiative decay rate to radiative rate (k_{nr}/k_r) in THF was dramatically decreased more than that in solid (6.12 vs 0.77), resulting from that the solid-environment retarded molecular motions. By contrast, the ratio for 2TPE-TD was increased in THF than that in solid (0.55 vs 2.25), implying that more nonradiative rate such as intermolecular π - π packing might still exist in solid. Undoubtedly, the antistacking of *spiro*-cyclohexane substituent on BI core played a significant role in suppressing nonradiative pathway to enhance solid-luminescence.

TD-DFT calculations at the cam-B3LYP/6-31G* level based on solvation of THF in the ground state (S_0) and excited state (S_1) were carried out so as to relate molecular structure to photo-physical property in solution (Figure 2A, and Figures S9–S15 and Tables S1–S3, S5, and S6 in the Supporting Information). Both electron densities of HOMO are distributed at the whole molecule by reason of that TPE is not a fine electron-donating group, whereas that of LUMO are located on the acceptor

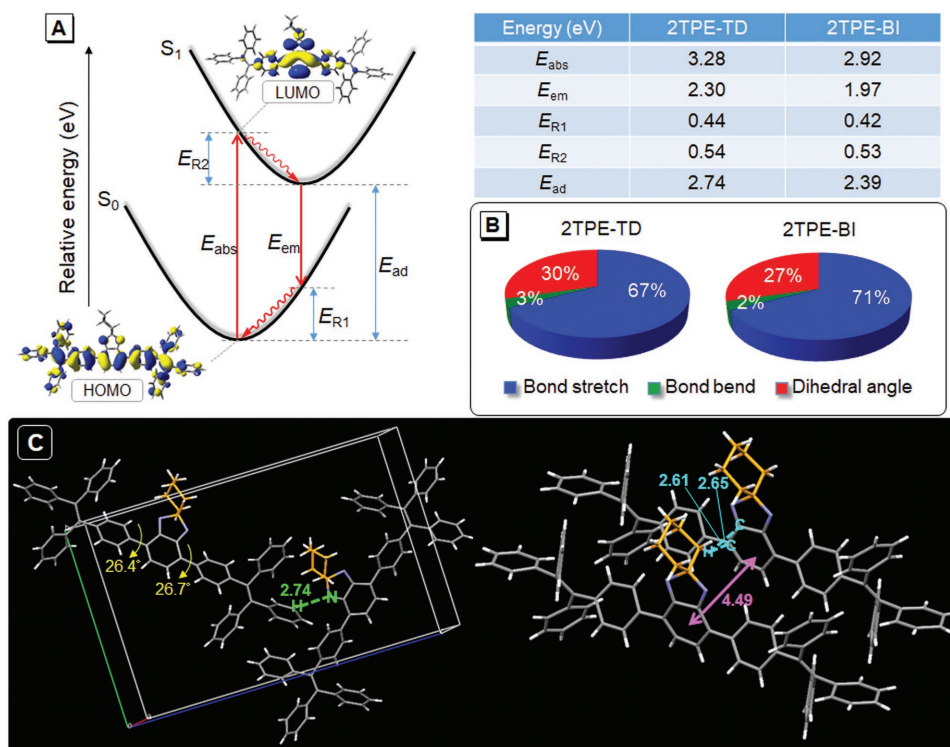


Figure 2. A) Schematic diagram of energy levels and their relative energy, where the inset is molecule orbitals of 2TPE-BI in S_0 state, calculated with TD-DFT as the level of cam-B3LYP/6-31G* based on solvation of THF. E_{abs} , E_{em} , E_{R1} , E_{R2} , and E_{ad} donate the energy difference of absorption from S_0 to S_1 states, that of emission from S_1 to S_0 states, that of relaxation in S_0 state, that of relaxation in S_1 state, and that between the minimum S_1 and S_0 states, respectively. B) The analyses of relative molecular motions according to the calculated reorganization energy of 2TPE-TD and 2TPE-BI in S_1 states, calculated with TD-DFT as the level of cam-B3LYP/6-31G* based on solvation of THF and then analyzed with MOMAP software. C) XRD crystallographic packing unit and structure of 2TPE-BI single crystal, where C atoms of cyclohexyl-substitution are marked with deep-yellow color, and the unit of bond distance is Å.

(BI and TD cores). Based on the similar dihedral angles between TPE and acceptor core for 2TPE-BI (−33.3 and 33.5°) and 2TPE-TD (−37.3 and 37.3°), 2TPE-BI has smaller energy gap than 2TPE-TD resulting from its stronger electron-withdrawing core. To further analyze the radiative decay rate, which is relative to spontaneous emission mainly and determined by the Einstein relationship^[26]

$$k_r = \frac{f \times \Delta E_{em}^2}{1.5} \quad (1)$$

where f and ΔE_{em} denote the oscillator strength and emission energy of the first transition at the S_1 geometry, respectively (Figure 2A), the calculated k_r value of 2TPE-BI (0.16 ns^{−1}) is about a half of that of 2TPE-TD (0.28 ns^{−1}), corresponding to the trend of the experimental results in THF solution. In addition, the main nonradiative decay pathway of excited fluorescent molecule is relative to the internal conversion rate (k_{IC}) between S_1 and S_0 states, which is determined by two important factors of the adiabatic excitation energy (E_{ad}) and reorganization energy (E_r). The E_{ad} values, defined the difference between the first excited-energy of S_1 state and the ground-energy of S_0 state, are 2.39 and 2.74 eV for 2TPE-BI and 2TPE-TD (Figure 2A), respectively. Smaller E_{ad} value for 2TPE-BI related to more k_{IC} was resulted from its stronger electron-deficient core (BI). On the other hand, through the analysis of the calculated E_r versus normal mode frequency (Figures S14 and S15, Supporting Information), the total reorganization energies (E_{rt}) are 463.73 and 452.01 meV for 2TPE-BI and 2TPE-TD, respectively. Projecting onto the internal coordinate (Figure 2B), the contributions for E_{rt} from bond stretch, bond bend and dihedral angle are little difference both. Although the vibrations of alkyl-chains appeared in the low-frequency region (<100 cm^{−1}) for 2TPE-BI, such motions are not the main influence on electron-vibration coupling of fluorescence decay in solution. Apparently, compared with 2TPE-TD, the smaller E_{ad} value of 2TPE-BI is the major reason for more fluorescence decay via nonradiative pathway, so that 2TPE-BI almost showed dim fluorescence in the solutions (Figure S5C, Supporting Information).

To further understand the relationship between molecular structure and AIE behavior, single crystal of 2TPE-BI was cultured by the mixture solvents of THF and hexane. According to the single crystal and packing structures (Figure 2C, and Figure S16 and Tables S7 and S8 in the Supporting Information), the molecular configuration of 2TPE-BI consisted of TPE, BI and the chair conformation of cyclohexyl-substitution. The bulky cyclohexane substituted on BI core and its peripheral TPE segments possess the steric hindrance, enabling to separate each molecule. The distance between the adjacent BI cores was 4.49 Å, which is long enough to prevent the intermolecular π - π interaction and ACQ phenomenon in the solid state. Besides, TPE segments mainly play the role of molecular rotators to consume the energy of the excited-molecule, leading to the weak emission in solution. Such intramolecular motions would be restricted by multiple intermolecular electrostatic interactions, such as C-H... π with distances in the range of 2.61–2.65 Å and C-H...N with distances of 2.74 Å in the crystalline state; at the same time, the molecular conformation would be also rigidified, and the dihedral angles between TPE and BI core

were reduced into 26.4° and 27.5°. The smaller dihedral angles than the calculated angles based on THF (vide supra) caused the better ICT and red-shifting photophysical properties in the solid state. These results brought about solid luminescence and AIE feature.

Cell surface glycans are involved in numerous physiological processes that involve cell-cell interactions and migration, including lymphocyte trafficking and cancer metastasis. *N*-acetyl-neuraminic-acid (sialic acid) is a natural component of the cell surface, in which cancer cells show a higher concentration of sialic acid in the cell membrane. When unnatural monosaccharides are treated to cells, the cells use them as building blocks and made their own glycan by intrinsic metabolic pathway. Previous researchers have found that synthetic *N*-acyl-modified D-mannosamines can be taken up by cells, efficiently metabolized to the respective *N*-acyl-modified neuraminic acids in vitro and in vivo, and further incorporated onto cell surface by the promiscuous sialic acid biosynthetic pathway. To target unnatural sialic acids with azido-groups, DBCO was chosen as a bio-orthogonal chemical group because of its high reactivity to azido-groups through copper-free click reactions. For in vivo application, an NIR emissive fluorophore, 2TPE-2T-BI, was developed by inserting thiophene into the framework of 2TPE-BI (Figure 3A). As the conjugation length was lengthened, 2TPE-2T-BI showed bathochromic absorption (568 nm) and emission (701 nm) in comparison with 2TPE-BI or 2TPE-2B-TD (Figures S17 and S18 in the Supporting Information and Table 1) in THF. In addition, it also performed the prominent AIE feature (Figure 3A) along with the addition of poor solvent (1,4-dioxane) fraction into the good solvent (dimethyl sulfoxide; DMSO). As shown in Figure 3B and Scheme S3 (Supporting Information), the DBCO-AIEdots were prepared by nanoprecipitation method using 2TPE-2T-BI as luminogen and DSPE-PEG and DSPE-PEG-DBCO as encapsulation matrices, where DSPE intertwined with 2TPE-2T-BI to form the hydrophobic core, and the hydrophilic PEG segment self-assembled to form the outer layer with DBCO functional groups on surface. The maximum absorption and emission peaks of DBCO-AIEdots were 572 and 710 nm, respectively, and both of bands could be tailing up to near infrared region (Figure 3C), which holds particular advantages of low excitation energy and autofluorescence in biological media.^[27] The DBCO-AIEdots had a large Stokes shift of 138 nm to greatly minimize the self-absorption,^[27b] that typically observed in conventional organic dyes. The transmission electron microscopy image and dynamic light scattering measurement indicated that DBCO-AIEdots are in spherical shape with an average size of ~85 nm (Figure 3D), which was suitable for blood circulation in vivo.^[28] Besides, no demonstrable inhibitory effect was observed on the growth of cervical cancer MCF-7 cells as DBCO-AIEdots was added to the culture media at high concentration of up to 18 mg L^{−1} (Figure S19, Supporting Information).

As shown in Figure 4, MCF-7 human breast cancer cells treated with unnatural monosaccharides (Ac4ManNAz) were labeled with azido chemical group, where cellular uptake of free Ac4ManNAz is very fast due to its four hydrophobic acyl groups could generate large number of azido-groups.^[29] The azido-sialic acid-labeled cell surface glycans were then reacted with DBCO-group on AIE dots through biorthogonal metal-free click

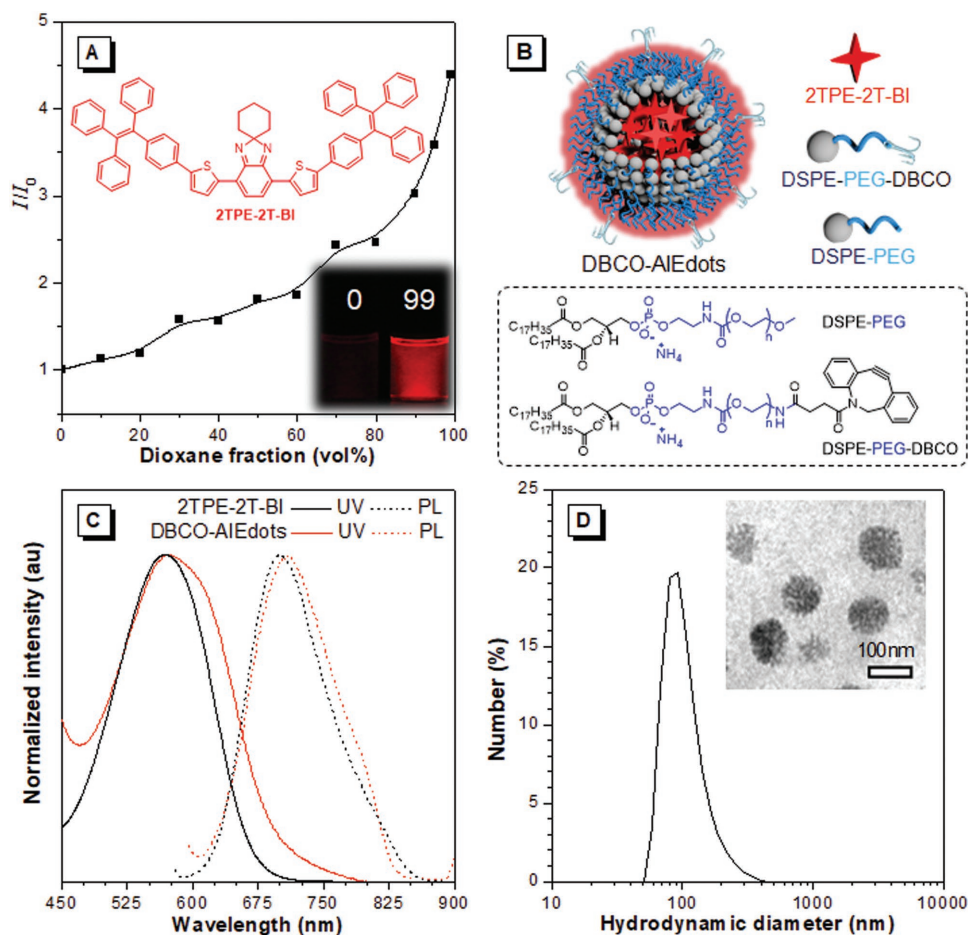


Figure 3. A) Plots of the relative emission intensity (I/I_0) versus the 1,4-dioxane fraction (f_D) of DMSO/1,4-dioxane mixtures of 2TPE-2T-BI, where the inset is the structure of 2TPE-2T-BI and the imaging of 0 and 99 vol% of f_D under UV light of 365 nm wavelength. B) Schematic illustration of bio-orthogonal DBCO-AIEdots structure, where the inset is the chemical structures of DSPE-PEG and DSPE-PEG-DBCO. C) Normalized UV-vis absorption and PL spectra of 2TPE-2T-BI and DBCO-AIEdots. D) Dynamic light scattering analysis of DBCO-AIEdots, where the inset is their transmission electron microscopy image.

chemistry.^[30] In this Ac4ManNAz-treated cell culture system, the binding of DBCO-AIEdots to the MCF-7 tumor cells was visualized by using confocal microscopy imaging. As shown in Figure 4B, MCF-7 cells treated with Ac4ManNAz showed strong red fluorescence intensity on the cell surface, indicating the successful expression of azido-groups. The control cells treated with phosphate buffer saline (PBS) and further incubated with DBCO-AIEdots, however, showed negligible fluorescence signals on the cell surface. These results collectively demonstrated that Ac4ManNAz was able to metabolically label MCF-7 cancer cells with azido-groups in vitro and visualized by bio-orthogonal DBCO-AIEdots.

Bio-orthogonal copper-free click chemistry also provided a safe and effective method for in vivo cell labeling and tracking. MCF-7 tumors were established in athymic nude mice by subcutaneous injection of MCF-7 cells into right flank. When the tumors reached $\approx 50 \text{ mm}^3$, Ac4ManNAz was administered into MCF-7 tumor bearing mice by intravenous injection once a day for 4 d, and then DBCO-AIEdots were injected via tail vein after 4 d. A time-dependent fluorescence of whole animal

NIR imaging approach was used to investigate the tumor targeting and in vivo distribution of DBCO-AIEdots in nude mice (Figure 4C). After DBCO-AIEdots delivered systemically for 12 h, the fluorescence signal for Ac4ManNAz-treated mouse was almost located around the tumor. By contrast, in the case of mouse without treatment of Ac4ManNAz, the fluorescence signal distributed almost all the body, indicating that the amount of accumulated DBCO-AIEdots in tumor tissue highly increased in the Ac4ManNAz-treated mouse in comparison with that in the saline-treated one due to the better bio-orthogonal copper-free click reaction with DBCO-AIEdots for the former. Finally, at 24 h postinjection, ex vivo tumors and other organs were dissected and analyzed in the Maestro in vivo imaging system (Figure 4D). As a result, it showed higher accumulation in tumor tissue for mouse treated with Ac4ManNAz. The amount of accumulated DBCO-AIEdots in tumor tissue highly increased in the Ac4ManNAz-treated mouse compared to the saline-treated one after intravenous injection of DBCO-AIEdots. After quantified the fluorescence signal, the reaction efficiency of this in vivo bio-orthogonal click chemistry

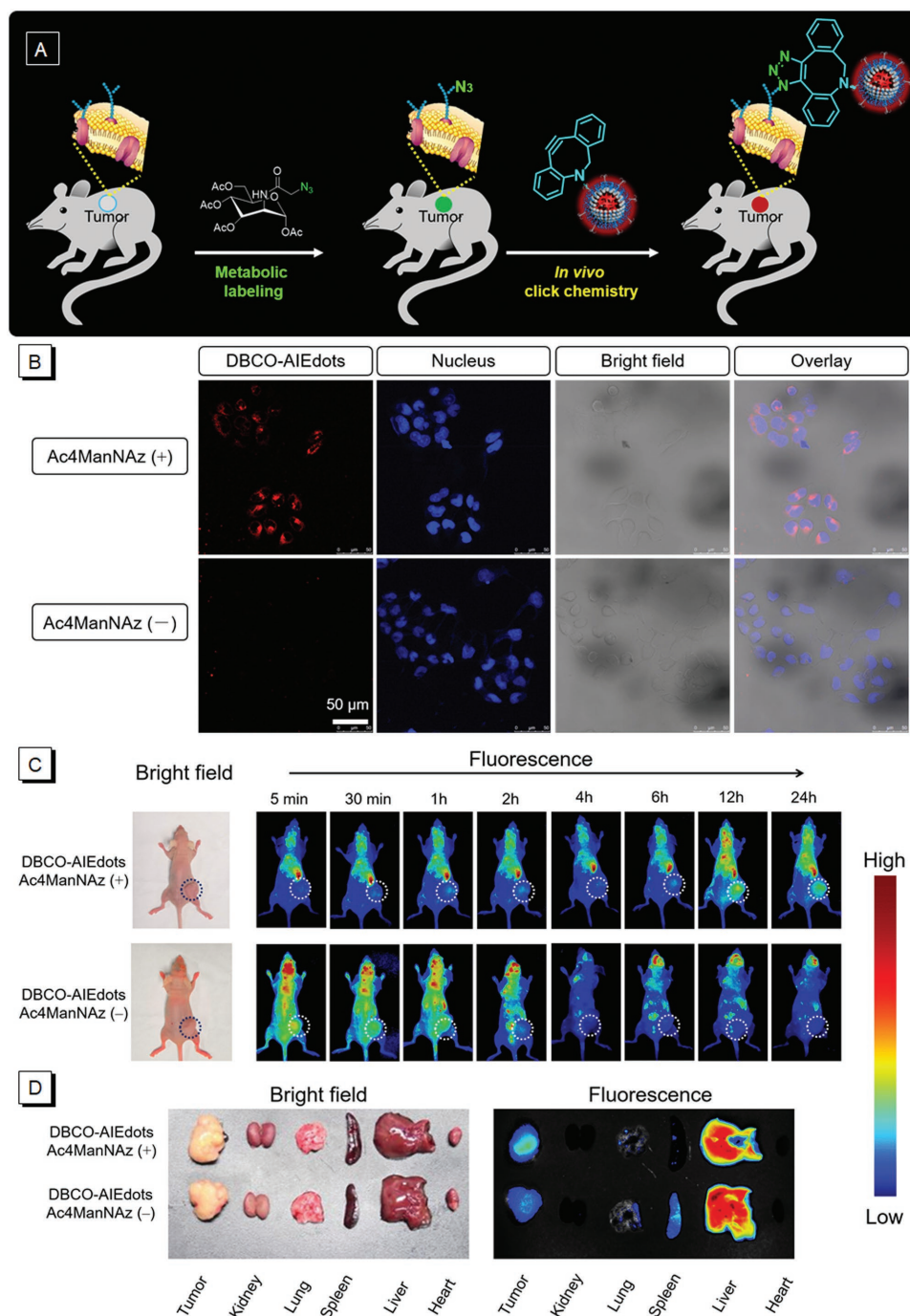


Figure 4. A) Schematic illustration of bio-orthogonal AIE-dots for in vivo metabolic labeling. B) Confocal laser scanning microscopy images of in vitro metabolic labeling for the MCF-7 cells by copper-free click chemistry after pretreatment of Ac4ManNAz. Excitation wavelength: 575 (DBCO-AIEdots) and 488 nm (nucleus probe, DAPI). Emission wavelength: 600-750 (DBCO-AIEdots) and 490-600 nm (DAPI). C) Time-dependent fluorescence images of in vivo tumor targeting imaging for metabolically labeled mouse injected with DBCO-AIEdots, whereas the mouse without Ac4ManNAz treatment was used as control. D) Ex vivo fluorescence images of organs and tumors in MCF-7 tumor-bearing mice after 24 h postinjection of DBCO-AIEdots. Excitation wavelength: 605 nm (DBCO-AIEdots). Emission wavelength: 640-900 (DBCO-AIEdots).

in tumor was about 21.34% (Figure S20, Supporting Information). The results showed that Ac4ManNAz could also label MCF-7 cancer cells in vivo and improve the tumor accumulation of AIE dots through bio-orthogonal click reaction, though

many nanoparticles were accumulated in the liver, which could be improved by using more cancer-selective metabolic labeling sugars^[19] or chemiluminescence probes.^[31] More importantly, compared with AIE dots with short wavelength emission, the

NIR emissive AIE dots showed higher contrast and signal to noise ratio for in vivo imaging due to the lower autofluorescence from the body (Figure S21, Supporting Information).

In summary, we introduced an electron-deficient BI core with a bulky cyclohexyl-substituent for developing orange-red and NIR AIEgens. The BI core efficiently avoids the intermolecular π - π stacking and meanwhile imparts its-based molecules with a high solubility and a D-A architecture. Compared with TD-based AIEgens, the present molecules showed enhanced AIE performances due to the stronger electron-withdrawing effect of the BI core and better intermolecular antistacking ability of the *spiro*-cyclohexane substituent. The DBCO-AIEdots with hydrophobic DSPE-segments, NIR-emissive AIEgens, hydrophilic PEG segments and clickable DBCO functional groups, exhibited red absorption and NIR emission with a large Stokes shift of 138 nm. By in vivo bio-orthogonal copper-free click reaction with the azido-groups of metabolic labeling tumor tissue, rapid tumor-specific imaging and real-time monitoring could be achieved. Compared with that for previous TD-based heterocycles, the present molecular design for long-wavelength emissive materials was not only simpler and more efficient in synthesis but also allowed to improve the AIE performance simultaneously. We believe that BI core and its derivatives will provide a new approach to design the competitive NIR materials. Such materials with NIR absorption and emission have great potential for in vivo photothermal and photodynamic therapy. More importantly, the excellent biocompatibility and high brightness of AIE dots will serve as imaging contrast agent for monitoring biomedical therapy process and image-guided surgery, and emerge as promising modalities for clinical applications.

[CCDC 1852708 contains the supplementary crystallographic data for this paper. These data can be obtained free of charge from The Cambridge Crystallographic Data Centre via www.ccdc.cam.ac.uk/data_request/cif]

Supporting Information

Supporting Information is available from the Wiley Online Library or from the author.

Acknowledgements

J.-S.N. and P.Z. contributed equally to this work. The authors are grateful for financial support from the Science and Technology Plan of Shenzhen (JCYJ20170307173739739 and JCYJ20160229205601482), the National Science Foundation of China (21788102, 21490570, 21490574, and 81501591), the Research Grants of Council of Hong Kong (16301614, 16305015, N_HKUST604/14, A-HKUST605/16, C2014-15G, and C6009-17G), the Innovation of Technology Commission (ITC-CNRC14SC01 and ITS/254/17), and China Postdoctoral Science Foundation (2016M602538 and 2018T110896). The authors also acknowledge the technical support received from AIEgen Biotech Co., Ltd. All animals used in these experiments received care in compliance with the guidelines outlined in the Guide for the Care and Use of Laboratory Animals. The procedures were approved by Shenzhen Institutes of Advanced Technology, Chinese Academy of Sciences Animal Care and Use Committee.

Conflict of Interest

The authors declare no conflict of interest.

Keywords

aggregation-induced emission, click reaction, donor-acceptor, in vivo metabolic labeling, near-infrared

Received: August 10, 2018

Revised: September 15, 2018

Published online: October 15, 2018

- [1] a) J. Huang, H. Nie, J. Zeng, Z. Zhuang, S. Gan, Y. Cai, J. Guo, S. J. Su, Z. Zhao, B. Z. Tang, *Angew. Chem., Int. Ed.* **2017**, *56*, 12971; b) F. Song, Z. Xu, Q. Zhang, Z. Zhao, H. Zhang, W. Zhao, Z. Qiu, C. Qi, H. Zhang, H. H. Y. Sung, I. D. Williams, J. W. Y. Lam, Z. Zhao, A. Qin, D. Ma, B. Z. Tang, *Adv. Funct. Mater.* **2018**, *28*, 1800051; c) F. Zhao, D. Ma, *Mater. Chem. Front.* **2017**, *1*, 1933.
- [2] F. De Nisi, R. Francischello, A. Battisti, A. Panniello, E. Fanizza, M. Striccoli, X. Gu, N. L. C. Leung, B. Z. Tang, A. Pucci, *Mater. Chem. Front.* **2017**, *1*, 1406.
- [3] a) J.-J. Liu, J. Yang, J.-L. Wang, Z.-F. Chang, B. Li, W.-T. Song, Z. Zhao, X. Lou, J. Dai, F. Xia, *Mater. Chem. Front.* **2018**, *2*, 1126; b) M. T. Gabr, F. Christopher Pigge, *Mater. Chem. Front.* **2017**, *1*, 1654; c) S. Gan, J. Zhou, T. A. Smith, H. Su, W. Luo, Y. Hong, Z. Zhao, B. Z. Tang, *Mater. Chem. Front.* **2017**, *1*, 2554; d) Q. Miao, C. Xie, X. Zhen, Y. Lyu, H. Duan, X. Liu, J. V. Jokerst, K. Pu, *Nat. Biotechnol.* **2017**, *35*, 1102.
- [4] a) Z. Guo, S. Park, J. Yoon, I. Shin, *Chem. Soc. Rev.* **2014**, *43*, 16; b) J. Qian, B. Z. Tang, *Chem* **2017**, *3*, 56; c) Q. Yang, Z. Ma, H. Wang, B. Zhou, S. Zhu, Y. Zhong, J. Wang, H. Wan, A. Antaris, R. Ma, X. Zhang, J. Yang, X. Zhang, H. Sun, W. Liu, Y. Liang, H. Dai, *Adv. Mater.* **2017**, *29*, 1605497.
- [5] L. Yuan, W. Lin, K. Zheng, L. He, W. Huang, *Chem. Soc. Rev.* **2013**, *42*, 622.
- [6] H. Nie, K. Hu, Y. Cai, Q. Peng, Z. Zhao, R. Hu, J. Chen, S.-J. Su, A. Qin, B. Z. Tang, *Mater. Chem. Front.* **2017**, *1*, 1125.
- [7] a) Y. Jiang, K. Pu, *Acc. Chem. Res.* **2018**, *51*, 1840; b) Q. Miao, K. Pu, *Adv. Mater.* **2018**, 1801778, <https://doi.org/10.1002/adma.201801778>.
- [8] a) I. McCulloch, R. S. Ashraf, L. Biniak, H. Bronstein, C. Combe, J. E. Donaghey, D. I. James, C. B. Nielsen, B. C. Schroeder, W. Zhang, *Acc. Chem. Res.* **2012**, *45*, 714; b) S. Holliday, Y. Li, C. K. Luscombe, *Prog. Polym. Sci.* **2017**, *70*, 34.
- [9] a) Z. Zhao, C. Deng, S. Chen, J. W. Lam, W. Qin, P. Lu, Z. Wang, H. S. Kwok, Y. Ma, H. Qiu, B. Z. Tang, *Chem. Commun.* **2011**, *47*, 8847; b) D. Ding, C. C. Goh, G. Feng, Z. Zhao, J. Liu, R. Liu, N. Tomczak, J. Geng, B. Z. Tang, L. G. Ng, B. Liu, *Adv. Mater.* **2013**, *25*, 6083.
- [10] a) X. Du, J. Qi, Z. Zhang, D. Ma, Z. Y. Wang, *Chem. Mater.* **2012**, *24*, 2178; b) B. Guo, Z. Sheng, D. Hu, C. Liu, H. Zheng, B. Liu, *Adv. Mater.* **2018**, *30*, 1802591; c) Z. Sheng, B. Guo, D. Hu, S. Xu, W. Wu, W. H. Liew, K. Yao, J. Jiang, C. Liu, H. Zheng, B. Liu, *Adv. Mater.* **2018**, *30*, 1800766.
- [11] a) Y. S. Yen, J. S. Ni, W. I. Hung, C. Y. Hsu, H. H. Chou, J. T. Lin, *ACS Appl. Mater. Interfaces* **2016**, *8*, 6117; b) L. Chen, L. Wang, X. Jing, F. Wang, *J. Mater. Chem.* **2011**, *21*, 10265.
- [12] M. Wang, X. Hu, P. Liu, W. Li, X. Gong, F. Huang, Y. Cao, *J. Am. Chem. Soc.* **2011**, *133*, 9638.

- [13] a) J. Qi, Y. Fang, R. T. K. Kwok, X. Zhang, X. Hu, J. W. Y. Lam, D. Ding, B. Z. Tang, *ACS Nano* **2017**, *11*, 7177; b) L. Wang, D. Cai, Q. Zheng, C. Tang, S.-C. Chen, Z. Yin, *ACS Macro Lett.* **2013**, *2*, 605; c) T. L. Tam, H. Li, Y. M. Lam, S. G. Mhaisalkar, A. C. Grimsdale, *Org. Lett.* **2011**, *13*, 4612; d) J. Qi, C. Sun, A. Zebibula, H. Zhang, R. T. K. Kwok, X. Zhao, W. Xi, J. W. Y. Lam, J. Qian, B. Z. Tang, *Adv. Mater.* **2018**, *30*, 1706856; e) X. Cai, J. Liu, W. H. Liew, Y. Duan, J. Geng, N. Thakor, K. Yao, L.-D. Liao, B. Liu, *Mater. Chem. Front.* **2017**, *1*, 1556.
- [14] a) J. Yu, J. L. Ornelas, Y. Tang, M. A. Uddin, H. Guo, S. Yu, Y. Wang, H. Y. Woo, S. Zhang, G. Xing, X. Guo, W. Huang, *ACS Appl. Mater. Interfaces* **2017**, *9*, 42167; b) D. T. T. Nguyen, T. Kim, Y. Li, S. Song, T. L. Nguyen, M. A. Uddin, S. Hwang, J. Y. Kim, H. Y. Woo, *J. Polym. Sci., Part A: Polym. Chem.* **2016**, *54*, 3826.
- [15] H. Li, S. Sun, S. Mhaisalkar, M. T. Zin, Y. M. Lam, A. C. Grimsdale, *J. Mater. Chem. A* **2014**, *2*, 17925.
- [16] a) J. Kim, S. H. Park, J. Kim, S. Cho, Y. Jin, J. Y. Shim, H. Shin, S. Kwon, I. Kim, K. Lee, A. J. Heeger, H. Suh, *J. Polym. Sci., Part A: Polym. Chem.* **2011**, *49*, 369; b) E. G. Cansu-Ergun, A. M. Önal, A. Cihaner, *Electrochim. Acta* **2016**, *188*, 165; c) S. Song, Y. Jin, S. H. Park, S. Cho, I. Kim, K. Lee, A. J. Heeger, H. Suh, *J. Mater. Chem.* **2010**, *20*, 6517.
- [17] a) X. Gu, E. Zhao, T. Zhao, M. Kang, C. Gui, J. W. Y. Lam, S. Du, M. M. T. Loy, B. Z. Tang, *Adv. Mater.* **2016**, *28*, 5064; b) J. Mei, J. W. Y. Lam, A. Qin, Y. Tang, B. Z. Tang, *Adv. Mater.* **2014**, *26*, 5429; c) F. Bu, R. Duan, Y. Xie, Y. Yi, Q. Peng, R. Hu, A. Qin, Z. Zhao, B. Z. Tang, *Angew. Chem., Int. Ed.* **2015**, *54*, 14492; d) X. Gu, X. Zhang, H. Ma, S. Jia, P. Zhang, Y. Zhao, Q. Liu, J. Wang, X. Zheng, J. W. Y. Lam, D. Ding, B. Z. Tang, *Adv. Mater.* **2018**, *30*, 1801065; e) G. Feng, B. Liu, *Acc. Chem. Res.* **2018**, *51*, 1404.
- [18] D. Mao, F. Hu, Kenry, S. Ji, W. Wu, D. Ding, D. Kong, B. Liu, *Adv. Mater.* **2018**, *30*, 1706831.
- [19] H. Wang, R. Wang, K. Cai, H. He, Y. Liu, J. Yen, Z. Wang, M. Xu, Y. Sun, X. Zhou, Q. Yin, L. Tang, I. T. Dobrucki, L. W. Dobrucki, E. J. Chaney, S. A. Boppart, T. M. Fan, S. Lezmi, X. Chen, L. Yin, J. Cheng, *Nat. Chem. Biol.* **2017**, *13*, 415.
- [20] M. Patra, K. Zarschler, H. J. Pietzsch, H. Stephan, G. Gasser, *Chem. Soc. Rev.* **2016**, *45*, 6415.
- [21] J. Lu, H. Yang, Y. Jin, Y. Jiang, H. Fu, *Green Chem.* **2013**, *15*, 3184.
- [22] M. Jiang, X. Gu, J. W. Y. Lam, Y. Zhang, R. T. K. Kwok, K. S. Wong, B. Z. Tang, *Chem. Sci.* **2017**, *8*, 5440.
- [23] J.-S. Ni, H. Liu, J. Liu, M. Jiang, Z. Zhao, Y. Chen, R. T. K. Kwok, J. W. Y. Lam, Q. Peng, B. Z. Tang, *Mater. Chem. Front.* **2018**, *2*, 1498.
- [24] a) S. Sasaki, S. Suzuki, W. M. Sameera, K. Igawa, K. Morokuma, G. Konishi, *J. Am. Chem. Soc.* **2016**, *138*, 8194; b) X. Liu, Q. Qiao, W. Tian, W. Liu, J. Chen, M. J. Lang, Z. Xu, *J. Am. Chem. Soc.* **2016**, *138*, 6960.
- [25] X. Zheng, Q. Peng, L. Zhu, Y. Xie, X. Huang, Z. Shuai, *Nanoscale* **2016**, *8*, 15173.
- [26] Z. Shuai, Q. Peng, *Natl. Sci. Rev.* **2017**, *4*, 224.
- [27] a) M. Gao, F. Yu, C. Lv, J. Choo, L. Chen, *Chem. Soc. Rev.* **2017**, *46*, 2237; b) P. Reineck, B. C. Gibson, *Adv. Opt. Mater.* **2017**, *5*, 1600446.
- [28] H. Wang, L. Tang, Y. Liu, I. T. Dobrucka, L. W. Dobrucki, L. Yin, J. Cheng, *Theranostics* **2016**, *6*, 1467.
- [29] H. Y. Yoon, H. Koo, K. Kim, I. C. Kwon, *Biomaterials* **2017**, *132*, 28.
- [30] M. K. Shim, H. Y. Yoon, J. H. Ryu, H. Koo, S. Lee, J. H. Park, J. H. Kim, S. Lee, M. G. Pomper, I. C. Kwon, K. Kim, *Angew. Chem., Int. Ed.* **2016**, *55*, 14698.
- [31] D. Mao, W. Wu, S. Ji, C. Chen, F. Hu, D. Kong, D. Ding, B. Liu, *Chem* **2017**, *3*, 991.